Review

Photoionization and Opacity

Anil Pradhan

Chemical Physics Program, Biophysics Graduate Program, Department of Astronomy, The Ohio State University, Columbus, OH 43210, USA; pradhan.1@osu.edu; Tel.: +1-614-292-5850

Abstract: Opacity determines radiation transport through material media. In a plasma source, the primary contributors to atomic opacity are bound–bound line transitions and bound-free photoionization into the continuum. We review the theoretical methodology for state-of-the-art photoionization calculations based on the R-matrix method as employed in the Opacity Project, the Iron Project, and solution of the heretofore unsolved problem of plasma broadening of autoionizing resonances due to electron impact, Stark (electric microfields), Doppler (thermal), and core-excitations. R-matrix opacity calculations entail huge amount of atomic data and calculations of unprecedented complexity. It is shown that in high-energy-density (HED) plasmas, photoionization cross sections become 3-D energy–temperature–density-dependent owing to considerable attenuation of autoionizing resonance profiles. Hence, differential oscillator strengths and monochromatic opacities are redistributed in energy. Consequently, Rosseland and Planck mean opacities are affected significantly.

Keywords: photoionization; opacity; autoionization; resonances; plasma broadening

1. Introduction

Physically, the opacity of an object depends on all possible intrinsic light–atom interactions that may absorb, scatter, or re-emit photons emanating from the source and received by the observer. In addition, the opacity depends on external conditions in the source and the medium. In recent years, there have been a number of theoretical and experimental studies of opacities (viz. [1–3]). Whereas photoionization and opacity are linked in all plasma sources, we focus specifically on high-energy-density (HED) environments such as stellar interiors and laboratory fusion devices, that are characterized by temperatures and densities together, typically $T > 10^6 K$ and densities $N > 10^{15}$ cm^{-3}. Computed atomic cross sections and transition proabilities are markedly perturbed by plasma effects.

Monochromatic opacity consist of four terms, namely, bound–bound (*bb*)), bound–free (*bf*), free–free (*ff*), and scattering (*sc*):

$$\kappa_{ijk}(\nu) = \sum_k A_k \sum_j F_j \sum_{i,i'}[\kappa_{bb(}(i,i';\nu) + \kappa_{bf}(i,\epsilon_i';\nu) + \kappa_{ff}(\epsilon_i,\epsilon_{i'}';\nu) + \kappa_{sc}(\nu)] . \quad (1)$$

In Equation (1), A_k is element abundance k, its ionization fraction F_j, i and initial bound and final bound/continuum states i, i', of a given atom; the ϵ represents electron energy in the continuum. To determine emergent radiation, a harmonic mean κ_R, is defined, Rosseland Mean Opacity (RMO), with monochromatic opacity $\kappa_{ijk}(\nu)$

$$\frac{1}{\kappa_R} = \frac{\int_0^\infty g(u)\kappa_\nu^{-1}du}{\int_0^\infty g(u)du} \quad \text{with} \quad g(u) = u^4 e^{-u}(1-e^{-u})^{-2}. \quad (2)$$

Here, $g(u)$ is the derivative of the Planck function including stimulated emission, $\kappa_{bb}(i,i') = (\pi e^2/m_e c)N_i f_{ii'}\phi_\nu$, and $\kappa_{bf} = N_i \sigma_\nu$. The κ_ν then depends on *bb* oscillator strengths, *bf*, photoionization cross sections σ_ν, on the equation-of-state (EOS) that gives level populations N_i. We describe large-scale computations using the coupled channel or

close coupling (hereafter CC) approximation implemented via the R-matrix (RM) method for opacity in Equation (1) primarily for: (i) the bb transition probabilities and (ii) the bf photoionization cross sections.

In this review, we focus on the bf-opacity, and in particular on resonant phenomena manifest in myriad series of autoionizing resonances that dominate photoionization cross sections throughout the energy ranges of interest in practical applications.

2. Photoionization

Photoionization (PI) of an ion X^{+z} with ion charge z into the (e + ion) continuum is

$$X^{+z} + h\nu \rightarrow X^{+z+1} + e. \tag{3}$$

PI also entails the indirect process of resonances via formation of autoionizing (AI) doubly excited states, and subsequent decay into the continuum, as

$$h\nu + X^{+Z} \rightleftharpoons (X^{+Z})^{**} \rightleftharpoons X^{+Z+1} + e \tag{4}$$
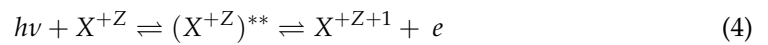
Infinite series of AI resonances are distributed throughout the photoionization cross section and generally dominate at lower energies encompassing and converging on to ionization thresholds corresponding to excited levels of the residual ion in the (e + ion) continua. A large number of photoionization cross-section values for all bound levels are needed to compute plasma opacities. Total photoionization cross section (σ_{PI}) of each bound level of the (e + ion) system are required, from the ground state as well as from all excited states. Practically, however, we consider $n(SLJ) < 10$, and approximate relatively small number of energies below thresholds. Total σ_{PI} corresponds to summed contribution of all ionization channels leaving the residual ion in the ground and various excited states.

AI resonances in photoionization cross sections are dissolved by plasma density and temperature, resulting in an enhanced continuum background, as discussed later. However, the strong and isolated resonances can be seen in absorption spectra. Moreover, a sub-class of AI resonances corresponding to strong dipole transitions within the core ion, known as Photoexcitation-of-core (PEC) or Seaton resonances, correspond to the inverse process of dielectronic recombination [4,5].

Transition matrix for photoionization $S = < \Psi_F || \mathbf{D} || \Psi_B >$ is obtained from bound and continuum wave functions which give the line strength using the expression above. Photoionization cross section is obtained as

$$\sigma_{PI} = \frac{4\pi}{3c} \frac{1}{g_i} \omega S, \tag{5}$$

where ω is the incident photon energy in Rydberg units.

2.1. The Opacity Project and R-Matrix Method

Astrophysical opacity calculations using the RM method were intitated under the Opacity Project (circa 1983) [4–7]. The RM opacity codes were developed to compute large-scale and accurate bound–bound (bb) transition oscillator strengths, and bound-free (bf) photoionization cross sections, Considerable effort was devoted to precise delineation of the *intrinsic* AI resonance profiles in terms of shapes, heights, energy ranges, and magnitudes determined by numerous coupled channels of the (e + ion) system.

In the CC-RM method, the total (e + ion) system is expressed in terms of the eigenfunctions of the target or core states and a free-electron

$$\Psi(E) = \mathcal{A} \sum_i \chi_i \theta_i + \sum_j c_j \Phi_j. \tag{6}$$

The χ_i are target ion wavefunctions in a specific $S_i L_i$ state, θ_i is the free-electron wavefunction, and Φ_j are bound channel correlation functions with coefficient c_j (viz. [4,5]). The

coupled channel labeled as $S_iL_ik_i^2\ell_i(SL\pi)$; k_i^2 is the incident kinetic energy. In contrast, the distorted wave approximation used in current opacity models neglects the summation over channels in Equation (6), and therefore coupling effects are not considered as in the RM method in an *ab initio* manner, due to possibly hundreds to thousands of coupled channels for complex ions. In principle, this approximation implies neglect of quantum superposition in the distorted wave method, and interference that manifests in autoionizing resonance profiles.

The bb, bf transition matrix elements for the (e + ion) wave functions $\Psi_B(SL\pi; E)$ and $\Psi_F(SL\pi; E')$, respectively, bound state B and B' line strengths (a.u.) are given by

$$S(B; B') = |\langle\Psi_B(E_B)||\mathbf{D}||\Psi_{B'}(E_{B'})\rangle|^2. \tag{7}$$

For opacity computations, we consider the $\mathbf{D}$ dipole operator, since non-dipole transitions do not generally act as significant contributors. With the final continuum state represented by $\Psi_F(E')$ and the initial state by $\Psi_B(E)$, the photoionization cross section is

$$\sigma_\omega(B; E') = \frac{4}{3}\frac{\alpha\omega}{g_i}|\langle\Psi_B(E_B)||\mathbf{D}||\Psi_F(E')\rangle|^2. \tag{8}$$

The ω is photon frequency and E' is the photoelectron energy of the outgoing electron. The Breit–Pauli R-matrix (BPRM) incorporates relativistic effects using the the Breit–Pauli (BP) Hamiltonian for the (e + ion) system in BPRM codes in intermediate coupling with a pair-coupling scheme $S_iL_l(J_i)l_i(K_i)s_i(J\pi)$ [8], whereby states S_iL_i split into fine-structure levels $S_iL_iJ_i$. Consequently, the number of channels becomes several times larger than the corresponding LS coupling case. The IP work is generally based on BPRM codes, as for example the large amount of radiative and collisional data in the database NORAD [9].

2.2. R-Matrix Calculations for Opacities

The *R*-Matrix codes employed in opacities calculations are considerably different and extensions of the original *R*-Matrix codes [4–6]. The OP codes were later extended under the Iron Project [10] to incorporate relativistic effects and fine structure in the Breit–Pauli approximation [8]. The RM opacity codes were further adapted with new extensions at Ohio State University for complete RM opacity calculations [3,11]. Figure 1 shows the flowchart of the RM codes at the Ohio Supercomputer Center (OSC). The atomic structure codes SUPERSTRUCTURE [12] and CIV3 [13], are first utilized to obtain an accurate configuration-interaction representation of the core-ion states. Next, the two *R*-Matrix codes STG1 and STG2 are employed to generate multipole integrals and algebraic coefficients for the (e + ion) Hamiltonian corresponding to coupled integro-differential equations in the CC approximation. In the BPRM codes, the code RECUPD recouples the LSJ pair coupling representation incluing fine structure explicitly. The total (e + ion) Hamiltonian matrix is diagonalized in STGH. The *R*-Matrix basis functions and dipole matrix elements thus obtained are input to code STGB for bound state wavefunctions B, code STGF for continuum wavefunctions, bb transitions code STGBB, and code STGBF to compute photoionization cross sections. Code STGF(J) may also be used to obtain electron impact excitation collision strengths.

THE R–MATRIX CODES AT OSU
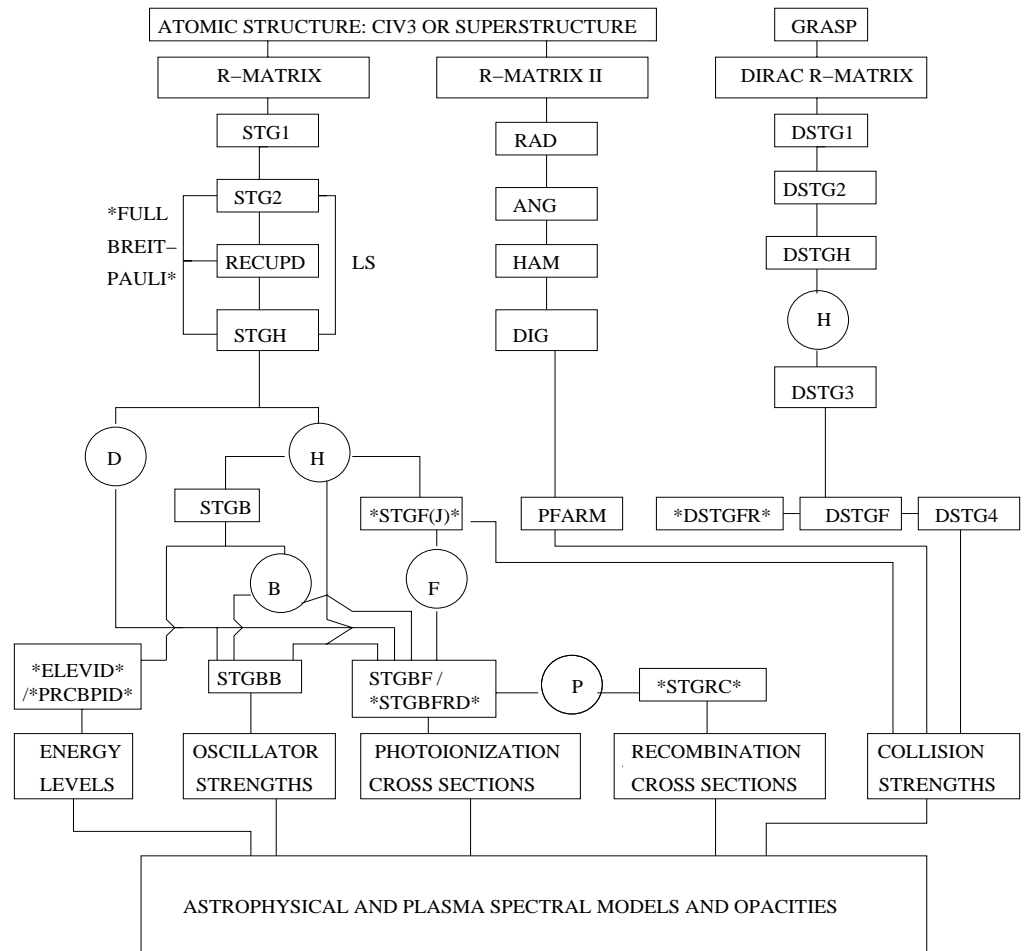
Figure 1. The R-matrix codes for opacities calculations (codes with * were developed or extended at OSU). Atomic data produced are further processed via a suite of equation-of-state, plasma broadening, and opacity codes to obtain monochromatic and mean opacities at each temperature and density [14].

The immense complexity of RM calculations, compared to DW method and atomic structure calculations, requires substantial computational effort and resources. In particular, inner-shell transitions are often dominant contributors to opacity. However, those could not be completed in OP work, except for outer-shell radiative transtions using the RM or BPRM methods due to computational constraints and then available high-performance computing platforms. Therefore, the simpler DW method was used for most of the OP opacity calculations, such as in DW-type methods in other opacity models that also neglect channel couplings and hence initio consideration of autoionizing resonances in the bound-free continua. A prominent exemplar is the extensive role of *photoexcitation-of-core* (PEC) resonances, or Seaton resonances [4,5], associated with strong dipole transitions (viz. [3,11] for Fe XVII).

Despite unprecedented effort and advances, the OP-RM work faced several then intractable difficulties that limited the scope of atomic calculations. Primarily, the limitations were due to computational constraints which, in turn, did not enable accounting for important physical effects and a complete RM calculation of atomic opacities. The main features and deficiencies of OP are as follows: (I) The calculations were in LS coupling neglecting relativistic fine structure. (II) The close coupling wavefunction expansion for the target or the core ion in the (e + ion) system included only a few ground configuration LS terms. (III) Inner-shell excitations could not be included owing to the restricted target-ion expansion that precluded

photoexcitation of levels from inner shells into myriad resonances in the continua of the residual (e + ion) system. (IV) Autoionizing resonances in bound-free photoionization cross sections were delineated within the few excited target terms. (V) Total angular and spin (e + ion) symmetries with large orbital angular-spin quantum numbers were not computed. All of these factors are crucial for a complete, converged and accurate opacity calculation. As mentioned, the OP work initially began with the *R*-matrix codes, albeit with very small wavefunction expansions (e + ion) system, usually limited to the ground configuration of the core ion. Thus, OP opacities incorporated a small subset of RM data. Rather, most of the opacities contributions were obtained using atomic structure codes and the Distorted Wave (hereafter DW) approximation, similar to other opacity models [5,6,9,10,15].

The first complete RM calculation leading up to the calculation of opacities was carried out for the ion Fe XVII that is of considerable importance in determining the opacity at the base of the solar convection zone (BCZ) ([11], hereafter NP16). The solar radius of the BCZ has been accurately determined through Helioseismology to be $0.713 \pm 0.001 \, R_\odot$.

Other new physical issues also emerged in RM calculations for opacities. There are three major problems that need to be solved: (A) Convergence of large-coupled channel wavefunction expansions necessary to include sufficient atomic structures manifest in opacity spectra. (B) Completeness of high $n\ell$ contributions up to $n \equiv \infty$, and (C) attenuation of resonance profiles due to *intrinsic* autoionization broadening (included in RM calculations in an ab initio manner) and *extrinsic* plasma effects due to temperature and density, as generally considered for bound–bound line opacity.

RM photoionization calculations have been carried for several Fe ions [16]. In particular, large-scale computations of cross sections and transition probabilities have been performed for Fe ions that determine iron opacity at the solar BCZ: Fe XVII, Fe XVIII, Fe XIX, Fe XX and Fe XXI (to be published; S.N. Nahar, private communication).

2.3. R-Matrix and Distorted Wave Methods

Current opacity models employ the DW approximation or variants thereof, based on an atomic structure calculation coupled to the continuum. Oscillator strengths and photoionization cross sections are computed for all possible bound–bound and bound-free transitions among levels specified by electronic configurations included in the atomic calculation. However, since the DW approximation includes only the coupling between initial and final states, the complexity of interference between the bound and continuum wavefunction expansions involving other levels is neglected, and so are the detailed profiles of autoionizing resonances embedded in the continua. DW models employ the independent resonance approximation that treats the bound–bound transition probability independently from coupling to the continuum. Apart from relative simplicity of atomic computations, the advantage of using DW models is that well-established plasma line broadening treatments may be used.

On the other hand, RM opacities calculations are computationally laborious and time-consuming. However, as demonstrated in the erstwhile OP-RM work, albeit severely limited in scope, coupling effects are important. Opacity in the bound-free continuum is dominated by autoionizing resonances, as shown in recently completed works (viz. [3,11,17]). The most important consequence of neglecting detailed resonance profiles in DW models and missing opacity is that *intrinsic* autoionizing broadening and *extrinsic* plasma broadening thereof are not fully accounted for. It has now been shown that AI resonances are broadened much wider in the continuum than lines, and thereby enhance opacity significantly [3,11].

Recent work ([18], D21) extended Fe XVII RM calculations by including more configurations than NP16a. Although this confirmed our earlier results for photoionization cross sections, D21 do not consider plasma broadening of autoionizing resonances and therefore do not obtain a complete description of bound-free opacity from RM calculations (discussed below).

The unbroadened cross sections in D21 appear similar to ours; however, they did not compare those in detail with previously published data in [11] for Fe XVII, and publicly available from the electronic database NORAD [9]. Furthermore, D21 report 10% lower Rosseland mean opacities than OP2005, which is at variance with other DW models that are higher by up to a factor of about 1.5 [3,11], possibly due to an incomplete number of bound Fe XVII levels.

3. Inner- and Outer-Shell Excitations

Being simpler and based on pre-specified electronic configurations as in atomic structure calculations, inner-shell excitation DW data may be readily computed treating resonances as bound levels in the continuum. Although OP opacities were computed using DW data, OP atomic codes were originally developed to implement the RM methodology that could not be carried through owing to computational constraints. Most importantly, it could not be employed for opacities due to inner-shell excitations that are dominant contributors because most electrons in complex ions are in closed shells and bear excitation energies that lie above the first ionization threshold, giving rise to series of autoionizing resonances, and in particular PEC resonances due to strong dipole inner-shell trasitions in the core ion [11,17]. On the other hand, the much simpler DW treatment in opacity models is readily implemented but is inaccurate in the treatment of important resonance phenomena. Extensive comparison of RM and DW calculations for Fe XVII considered herein, and implications for plasma opacities, are given in [11,19].

4. Plasma Broadening of Resonances

Whereas line broadening has long been studied and its treatments are generally and routinely incorporated in opacity models (viz. [4]), plasma broadening of autoionizing resonance profiles is not heretofore considered. Attenuation of shape, height, energies, and magnitude of autoionizing resonances in photoionization cross sections must be delineated in detail, as in the RM method, as a function of density and temperature in order to determine the distribution of total differential oscillator strength and structure of the bound-free continua.

AI resonances are fundamentally different from bound–bound lines as related to quasi-bound levels with *intrinsic* quantum mechanical autoionization widths. Broadening has significant contribution to mean opacities, enhancing the Rosseland mean opacity by factors ranging from 1.5 to 3, as shown in other works and discussed below [17]. However, line-broadening processes and formulae may be to develop a theoretical treatment and computational algorithm outlined herein (details to be presented elsewhere). The convolved bound-free photoionization cross section of level *i* may be written as:

$$\sigma_i(\omega) = \int \tilde{\sigma}(\omega')\phi(\omega',\omega)d\omega', \tag{9}$$

where σ and $\tilde{\sigma}$ are the cross sections with plasma-broadened and unbroadened AI resonance structures, ω is the photon energy (Rydberg atomic units are used throughout), and $\phi(\omega',\omega)$ is the normalized Lorentzian profile factor in terms of the *total* width Γ due to all AI broadening processes included:

$$\phi(\omega',\omega) = \frac{\Gamma(\omega)/\pi}{x^2 + \Gamma^2}, \tag{10}$$

where $x \equiv \omega - \omega'$. The crucial difference with line broadening is that AI resonances in the (e + ion) system correspond to and are due to quantum mechanical interference between discretized continua defined by excited core ion levels in a multitude of channels. The RM

method (viz. [4–6]), accounts for AI resonances in an (e + ion) system with generally asymmetric profiles (unlike line profiles that are usually symmetric).

Given N core-ion levels corresponding to resonance structures,

$$\sigma(\omega) = \sum_i^N \left[\int \tilde{\sigma}(\omega') \left[\frac{\Gamma_i(\omega)/\pi}{x^2 + \Gamma_i(\omega)} \right] d\omega' \right]. \tag{11}$$

With $x \equiv \omega' - \omega$, the summation is over all excited thresholds E_i included in the N-level RM wavefunction expansion, and corresponding to total damping width Γ_i due to all broadening processes. The profile $\phi(\omega', \omega)$ is centered at each continuum energy ω, convolved over the variable ω' and relative to each excited core ion threshold i. In the present formulation we associate the energy to the effective quantum number relative to each threshold $\omega' \to \nu_i$ to write the total width as:

$$\begin{aligned} \Gamma_i(\omega, \nu, T, N_e) &= \Gamma_c(i, \nu, \nu_c) + \Gamma_s(\nu_i, \nu_s^*) \\ &+ \Gamma_d(A, \omega) + \Gamma_f(f - f; \nu_i, \nu_i'), \end{aligned} \tag{12}$$

pertaining to collisional Γ_c, Stark Γ_s, Doppler Γ_d, and free–free transition Γ_f widths respectively, with additional parameters as defined below. We assume a Lorentzian profile factor that subsumes both collisional broadening due to electron impact, and Stark broadening due to ion microfields, that dominate in HED plasmas. This approximation should be valid since collisional profile wings extend much wider as x^{-2}, compared to the shorter range $exp(-x^2)$ for thermal Doppler, and $x^{-5/2}$ for Stark broadening (viz. [4,17]). In Equation (11), the limits $\mp\infty$ are then replaced by $\mp\Gamma_i/\sqrt{\delta}$; δ is chosen to ensure the Lorentzian profile energy range for accurate normalization. Convolution by evaluation of Equations (1)–(3) is carried out for each energy ω throughout the tabulated mesh of energies used to delineate all AI resonance structures, for each cross section, and each core ion threshold. We employ the following expressions for computations:

$$\Gamma_c(i, \nu) = 5\left(\frac{\pi}{kT}\right)^{1/2} a_o^3 N_e G(T, z, \nu_i)(\nu_i^4/z^2), \tag{13}$$

where T, N_e, z, and A are the temperature, electron density, ion charge and atomic weight, respectively, and ν_i corresponds to a given core ion threshold $i : \omega \equiv E = E_i - \nu_i^2/z^2$ is a continuous variable. The Gaunt factor [17] $G(T, z, \nu_i) = \sqrt{3}/\pi[1/2 + ln(\nu_i kT/z)]$ Another factor $(n_x/n_g)^4$ is introduced for Γ_c to allow for doubly excited AI levels with excited core levels n_x relative to the ground configuration n_g (e.g., for Fe XVIII $n_x = 3, 4$ relative to the ground configuration $n_g = 2$). A treatment of the Stark effect for complex systems entails two approaches, one where both electron and ion perturbations are combined, or separately (viz. [4,17]) employed herein. Excited Rydberg levels are nearly hydrogenic, the Stark effect is linear and ion perturbations are the main broadening effect, though collisional broadening competes increasingly with density as ν_i^4 (Equation (13)). The total Stark width of a given n-complex is $\approx(3F/z)n^2$, where F represents the plasma electric microfields. Assuming the dominant ion perturbers to be protons and density equal to electrons, we take $F = [(4/3)\pi a_o^3 N_e)]^{2/3}$, consistent with the Mihalas–Hummer-Däppen equation-of-state formulation [4].

$$\Gamma_s(\nu_i, \nu_s^*) = [(4/3)\pi a_o^3 N_e]^{2/3} \nu_i^2. \tag{14}$$

In employing Equation (12), a Stark ionization parameter $\nu_s^* = 1.2 \times 10^3 N_e^{-2/15} z^{3/5}$ is introduced such that AI resonances may be considered fully dissolved into the continuum for $\nu_i > \nu_s^*$ (analogous to the Inglis–Teller series limit for plasma ionization of bound levels). Calculations are carried out with and without ν_s^*, as shown in [17]. The Doppler width is:

$$\Gamma_d(A, T, \omega) = 4.2858 \times 10^{-7} \sqrt{(T/A)}, \tag{15}$$

where ω is *not* the usual line center but taken to be each AI resonance energy. The last term Γ_f in Equation (5) accounts for free–free transitions among autoionizing levels with v_i, v_i' such that

$$X_i + e(E_i, v_i) \longrightarrow X_i' + e'(E_i', v_i'). \tag{16}$$

The large number of free–free transition probabilities for $+ve$ energy AI levels $E_i, E_i' > 0$ may be computed using RM or atomic structure codes (viz. [20]).

We utilize new results from an extensive Breit–Pauli R-Matrix (BPRM) calculation with 218 fine structure levels dominated by $n \leq 4$ levels of the core ion Fe XVIII (to be reported elsewhere). A total of 587 Fe XVII bound levels ($E < 0$) are considered, dominated by configurations $1s^2 2s^2 2p^6 (^1S_0), 1s^2 2s^p 2p^q n\ell, [SLJ]$ ($p, q = 0 - -2$, $n \leq 10$, $\ell \leq 9$, $J \leq 12$). The core Fe XVII levels included in the RM calculation for the (e + Fe XVIII) →Fe XVII system are: $1s^2 2s^2 2p^5 (^2P^o_{1/2,3/2}), 1s^2 2s^2 2p^q, n\ell, [S_i L_i J_i]$ ($p = 4, 5$, $n \leq 4, \ell \leq 3$). The Rydberg series of AI resonances correspond to $(S_i L_i J_i)\, n\ell$, $n \leq 10, \ell \leq 9$, with effective quantum number defined as a continuous variable $v_i = z/\sqrt{(E_i - E)}$ ($E > 0$), throughout the energy range up to the highest 218th Fe XVIII core level; the $n = 2, 3, 4$ core levels range from $E = 0$–90.7 Ry ([11]). The Fe XVII BPRM calculations were carried out resolving the bound-free cross sections at $\sim$40,000 energies for 454 bound levels with AI resonance structures. Given 217 excited core levels of Fe XVIII, convolution is carried out at each energy or approximately 10^9 times for each (T, N_e) pair.

Figure 2 displays detailed results for unbroadened photoionization cross section (black) and plasma broadened (red and blue, without and with Stark ionization cut-off) The excited bound level of Fe XVII is $2s^2 2p^2\, ^3D_2$ at temperature–density $T = 2 \times 10^6$ K and $N_e = 10^{23}$ cm^{-3}. The cross section is shown on the Log_{10} scale in the top panel, and on a linear scale in the bottom panel isolating the energy region of highest and strongest AI resonances. The main features evident in the figure are as follows. (i) AI resonances show significant plasma broadening and smearing of a multitude of overlapping Rydberg series at The narrower high-nl resonances dissolve into the continua but stronger low-nl resonance retain their asymmetric shapes with attenuated heights and widths. (ii) At the $N_e = 10^{23}$ cm^{-3}, close to that at the solar BCZ, resonance structures not only broaden but their strengths shift and are redistributed over a wide range determined by total width $\Gamma(\omega, v_i, T, N_e)$ at each energy $\hbar\omega$ (Equation (12)). (iii) Stark ionization cut-off (blue curve) results in step-wise structures that represent the average due to complete dissolution into continua. (iv) Integrated AI resonance strengths are conserved, and are generally within 5–10% of each other for all three curves in Figure 2. It is found that the ratio of RMOs with and without plasma broadening may be up to a factor of 1.6 or higher ([17]); recent work for other ions shows the ratio may be up to factor of 3.

The scale and magnitude of new opacity calculations is evident from the fact that photoionization cross sections of 454 bound levels of Fe XVII are explicitly calculated using the RM opacity codes, 1154 levels of Fe XVIII, and 899 levels Fe XIX. Plasma broadening is then carried out for for each temperature and density of interest throughout the solar and stellar interiors or HED plasma sources.
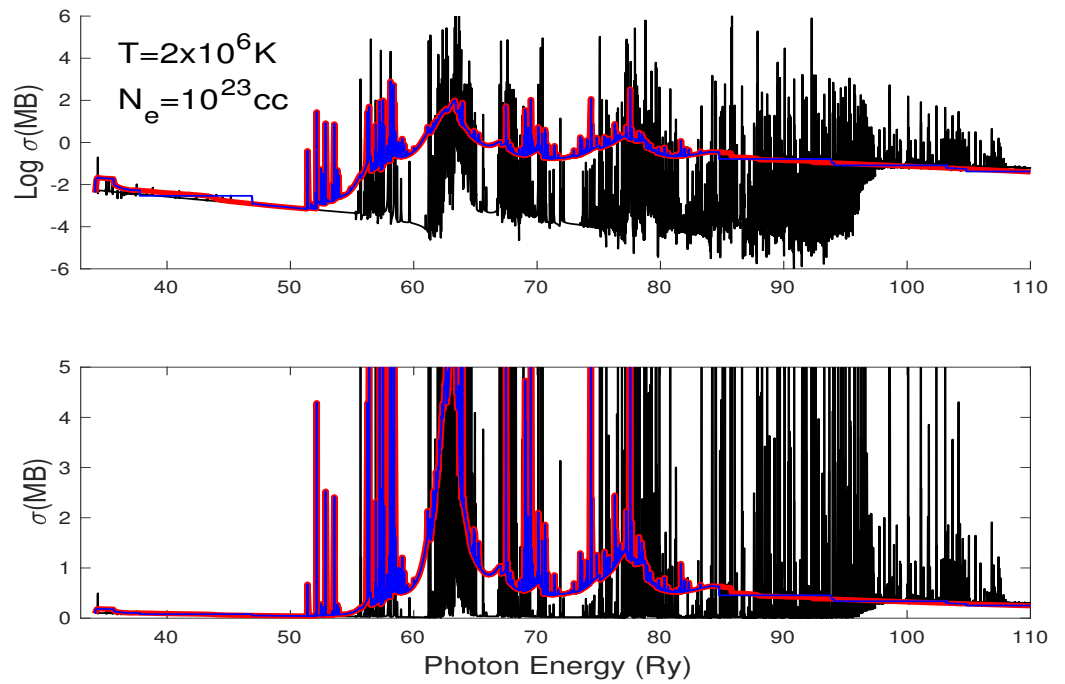
Figure 2. Energy–temperature–density-dependent photoionization cross section of highly excited bound level $2s^2 2p^5 3p \, ^2D_2$ of Fe XVII $\longrightarrow$ e + Fe XVIII, due to plasma broadening of autoionizing resonances: unbroadened—black curve, broadened—red and blue (see text). Top panel: Logσ (MB) in the full energy range up to the highest ionization threshold of core ion Fe XVIII, bottom panel: Linear-scale σ_{PI} in the energy range of the largest AI structures.

5. Energy Dependence

Photoionization cross sections vary widely in different approximations used to calculate opacities. Simple methods such as the *quantum defect method* and the central-field approximation, yield a feature-less background cross section. High-n levels in a Rydberg series of levels behave hydrogenically at sufficiently high energies, and the photoionization cross section may be approximated using Kramer's formula (discussed in [5])

$$\sigma_{PI} = \frac{8\pi}{3^{1.5}c} \frac{1}{n^5 \omega^3}. \tag{17}$$

Equation (17) is used in OP work to extrapolate photoionization cross sections in the high-energy region. However, it is not accurate, as seen in Figure 3. At high energies, inner shells and sub-shells are ionized, and their contribution must also be included in total photoionization cross sections. At inner (sub-)shell ionization thresholds, there is a sharp upward jump or edge and enhancement of the photoionization cross section. Figure 3 shows results from a relativistic distorted wave (RDW) calculation and Kramer's fomula Equation (17). The RDW results do not include resonances, and differ from the OP results with resonance structures in the relatively small energy region near the ioniization threshold.
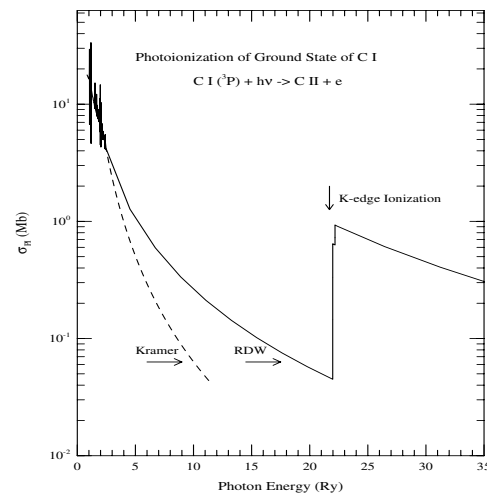
Figure 3. Photoionization cross section σ_{PI} of the ground state of CI, $1s^2 2s^2 2p^2 \, {}^3P$, computed using the relativistic distorted wave (RDW) code by H.L. Zhang (discussed in [5]) compared with the Kramer's hydrogenic formula Equation (17). The large jump is due to photoionization of the inner $1s-$shell or the K$-$edge. The resonance structures at very low energies are obtained from the coupled channel RM calculations in the Opacity Project.

6. From Convergence to Completeness

The NP16 work [11] also addressed an important point that a reasonably complete expansion of target configurations and levels in BPRM photoionization calculations is necessary to ensure converged bound-free opacities. The criteria for accuracy and completeness are: (i) *convergence* of the wavefunction expansion (Equation (6)), and (ii) *completeness* of PI cross sections, monochromatic and mean opacities with respect to possibly large number of multiply excited configurations.

While NP16 demonstrated convergence with respect to n = 2, 3, 4 levels of the Fe XVIII target ion included in the RM calculations, more highly excited configurations that might affect high-energy behavior were not included. Subsequent work using and comparing with the DW method was therefore carried out to ascertain the effect of high-$n\ell$ configurations on opacities [20].

Specifying excited configurations is straightforward in an atomic structure-DW calculation, but it is more complex and indirect in RM calculations. For example, in order to investigate the role of more excited configurations the NP16 BPRM calculations that yield 454 bound levels for Fe XVII, were complemented with >50,000 highn, ℓ "topup" levels to compute opacities and RMOs. Photoionization cross sections of the 454 strictly bound levels computed (negative eigenenergies) take into account embedded autoionizing resonances that are treated as distinct levels in DW calculations; therefore, in total there are commensurate number of levels to ensure completeness.

However, the large number of highly excited configurations made only a small contribution to opacities, relative to the main BPRM cross sections, and only to the background cross sections. without resonances. Therefore, the simpler DW method may be used for topup contributions without loss of accuracy as to supplement RM calculations. Recent work has shown that the topup contribution to RM opacities does not exceed 5% to RMOs [14].

7. Sum Rule and Oscillator Strength Distribution

The total *bb* and integrated *bf* oscillator strength, when summed over all possible bb and bf transitions, must satisfy the definition of the oscillator strength as fractional excitation probability, i.e., $\sum_j f_{ij} = N$, where N is the number of active electrons. However, while the f-sum rule ensures completeness, it does not ensure accuracy of atomic calculations *per se*. That depends on the precise energy distribution of differential oscillator df/dE,

strength or photoionization cross section σ_{PI}. To wit: the hydrogenic approximation, if used for complex atoms would satisfy the f-sum rule but would clearly be inaccurate. As discussed herein, the RM method is concerned primarily with df/dE in the bf-continuum based on full delineation of autoionizing resonance profiles.

As an end result, the RMO depends on energy distribution of monochromatic opacity, convolved over the Planck function at a given temperature. Compared with OP results, the distribution of RM Fe XVII monochromatic opacity is quite different, and much more smoothed out without sharp variations that stem mainly from the treatment of resonances as bb lines, even with limited autoionization broadening included perturbatively in DW opacity models. Experimentally, a flatter opacity distribution is also observed, in contrast to theoretical opacity models that exhibit larger dips in opacity at "opacity windows" [3,11,21,22].

8. Conclusions

This review describes photoionization work related to opacities. The state-of-the-art R-matrix calculations are discussed in comparison with the distorted wave data currently employed in opacity models. Atomic and plasma effects such as channel coupling, broadening of autoionizing resonances, high-energy behavior, and oscillator strength sum-rule are described.

Existing OP and IP radiative data for photoionization and transition probabilities for astrophysically abundant elements have been archived in databases TOPbase and TIPbase. OP opacities and radiative accelerations are available online from OPserver [15]. R-matrix data for nearly 100 atoms and ions from up-to-date and more accurate calculations are available from the database NORAD at OSU [9].

Data Availability Statement: All data reported in this work is available from the database NORAD [9] created by S.N. Nahar and maintained at the Ohio State University.

Conflicts of Interest: The author declares no conflict of interest.

References

1. Mendoza, C. Computation of Atomic Astrophysical Opacities. *Atoms* **2018**, *6*, 28. [CrossRef]
2. Pain, J.-C.; Croset, P. Ideas and Tools for Error Detection in Opacity Databases. *Atoms* **2023**, *11*, 27. [CrossRef]
3. Pradhan, A.K. Recalculation of Astrophysical Opacities: Overview, Methodology, and Atomic Calculations.In Proceedings of the Workshop on Astrophysical Opacities, Kalamazoo, MI, USA, 1–4 August 2017; Volume 515, pp. 79–88.
4. *The Opacity Project*; The Opacity Project Team, Institute of Physics Publishing: Bristol, UK, 1995; Volume 1.
5. Pradhan, A.K.; Nahar, S.N. *Atomic Astrophysics and Spectroscopy*; Cambridge University Press: Cambridge, UK, 2011.
6. *R-Matrix Theory of Atomic Collisions*; Springer Series on Atomic, Optical and Plasma Physics; Springer: Berlin/Heidelberg, Germany, 2011.
7. Seaton, M.J.; Yu, Y.; Mihalas, D.; Pradhan, A.K. Opacities for Stellar Envelopes. *Mon. Not. R. Astr. Soc.* **1994**, *266*, 805. [CrossRef]
8. Berrington, K.A.; Eissner, W.; Norrington, P.H. RMATRIX1: Belfast atomic R-matrix codes. *Comput. Phys. Commun.* **1995**, *92*, 290–420. [CrossRef]
9. Nahar, S.N. NORAD: Nahar-OSU-Radiative-Atomic-Data, The Ohio State University. Available online: http://norad.astronomy.osu.edu (accessed on 4 February 2023).
10. Hummer, D.G.; Berrington, K.A.; Eissner, W.; Pradhan, A.K.; Saraph, H.E.; Tully, J.A. Atomic data from the IRON Project. 1: Goals and methods. *Astron. Astrophys.* **1993**, *279*, 298–309.
11. Nahar, S.N.; Pradhan, A.K. Large Enhancement in high-energy photoionization of Fe XVII and missing continuum plasma opacity. *Phys. Rev. Lett.* **2016**, *116*, 249502–294507. [CrossRef] [PubMed]
12. Eissner, W.; Jones, M.; Nussbaumer, H. Techniques for the calculation of atomic structures and radiative data including relativistic corrections. *Comput. Phys. Commun.* **1974**, *8*, 270–306. [CrossRef]
13. Hibbert, A. CIV3—A general program to calculate configuration interaction wave functions and electric-dipole oscillator strengths. *Comput. Phys. Commun.* **1975**, *9*, 141. [CrossRef]

14. Pradhan, A.K.; Nahar, S.N.; Eissner, W.; Zhao, L. Chemical Physics Program, Biophysics Graduate Program. Department of Astronomy, The Ohio State University: Columbus, OH, USA, 2023; *manuscript in preparation*.
15. Mendoza, C.; Seaton, M.J.; Buerger, P.; Bellorin, P.; Melendez, M.; Gonzalez, J.; Rodriguez, L.S.; Palacios, E.; Pradhan, A.K.; Zeippen, C.J. Interactive online computations of opacities and radiative accelerations. *Mon. Not. R. Astron. Soc.* **2007**, *378*, 1031. Available online: http://cdsweb.u-strasbg.fr/topbase/topbase.html (accessed on 5 February 2023). [CrossRef]
16. Nahar, S.N. The IRON Project: Photoionization of Fe Ions. *ASP Conf. Ser.* **2018**, *515*, 93–103.
17. Pradhan, A.K. Plasma Broadening of Autoionzing Resonances. 2023. Available online: https://arxiv.org/pdf/2301.07734.pdf (accessed on 6 February 2023).
18. Delahaye, F.D.; Ballance, C.P. Smyth RT and Badnell NR, Quantitative comparison of opacities calculated using the R-matrix methods: Fe XVII. *Mon. Not. R. Astr. Soc.* **2021**, *508*, 421–432. [CrossRef]
19. Nahar, S.N.; Pradhan, A.K.; Chen, G.-X.; Eissner, W. Highly Excited Core Resonances in Photoionization of Fe XVII: Implications for Plasma Opacities. *Phys. Rev. A* **2011**, *83*, 053417. [CrossRef]
20. Zhao, L.; Eissner, W.; Nahar, S.N.; Pradhan, A.K. Converged R-matrix calculations of the Photoionization of Fe XVII in Astrophysical Plasmas: From Convergence to Completeness. *ASP Conf. Ser.* **2018**, *515*, 89–92.
21. Bailey, J.E.; Nagayama, T.; Loisel, G.P.; Rochau, G.A.; Blancard, C.; Colgan, J.; Cosse, P.; Faussurier, G.; Fontes, C.J.; Gilleron, F.; et al. A higher-than-predicted measurement of iron opacity at solar interior temperatures. *Nature* **2015**, *517*, 56–59. [CrossRef] [PubMed]
22. Nagayama, T.; Bailey, J.; Loisel, G.; Dunham, G.; Rochau, G.; Blancard, C.; Colgan, J.; Cossé, P.; Faussurier, G.; Fontes, C.; et al. Systematic Study of L-Shell Opacity at Stellar Interior Temperatures. *Phys. Rev. Lett.* **2019**, *122*, 235001. [CrossRef] [PubMed]